

Supporting Information

Molecular Sieve Properties of Carbon Silica Materials (CSM)

F. de Clippel, A. Harkiolakis, T. Vosch, G.V. Baron, P.A. Jacobs, J.F.M. Denayer*, B. F. Sels*

Nomenclature of the CSMs

- CSM-19 for instance presents a carbon silica material (CSM) that has been prepared according to the procedure in the main text using an impregnation solution of 50 Vol% of FA in mesitylene, corresponding to 19 wt% of carbon as measured by TGA under O₂.

Al-MCM-41 template material

- The diameter of a random selection of 50 spherical particles was measured using Coreldraw 8.0 software and the reference scale provided by the SEM equipment. As such, the size distribution of the Al-MCM-41 particles could be estimated, and is presented in **Figure 1**.
- The distribution was then fitted with a Gauss (Normal) plot using OriginPro 7.5 software. The following parameters were determined:
 - Mean diameter: 421 nm
 - Standard deviation: 106 nm

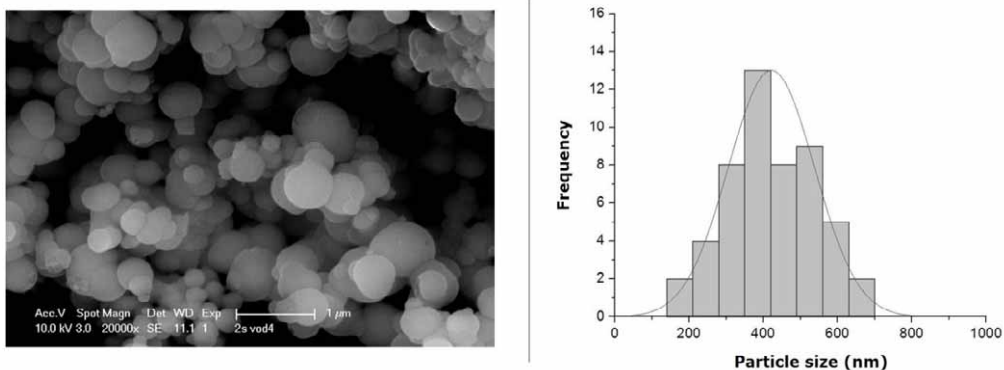


Figure 1: (left) SEM image of the parent Al-MCM-41 material; (right) Size distribution of the silica particles.

XRD diffractogram

The graphite crystallite size was estimated from the (002) indexed reflection peak of nanographite (at 23.5 2theta) using the Debye-Scherrer relationship:

$$\tau = \frac{K\lambda}{\beta \cos \Theta}$$

– Mean crystallite dimension:

- K = shape factor = 0.9
 - λ = X-ray wavelength = 1,54 Angström
 - β = FWHM = 0.157 rad (**Figure 2**)
 - Θ = Bragg Angle = 11.75° = 0.205 rad (**Figure 2**)
- $\tau = 9,08$ Angström

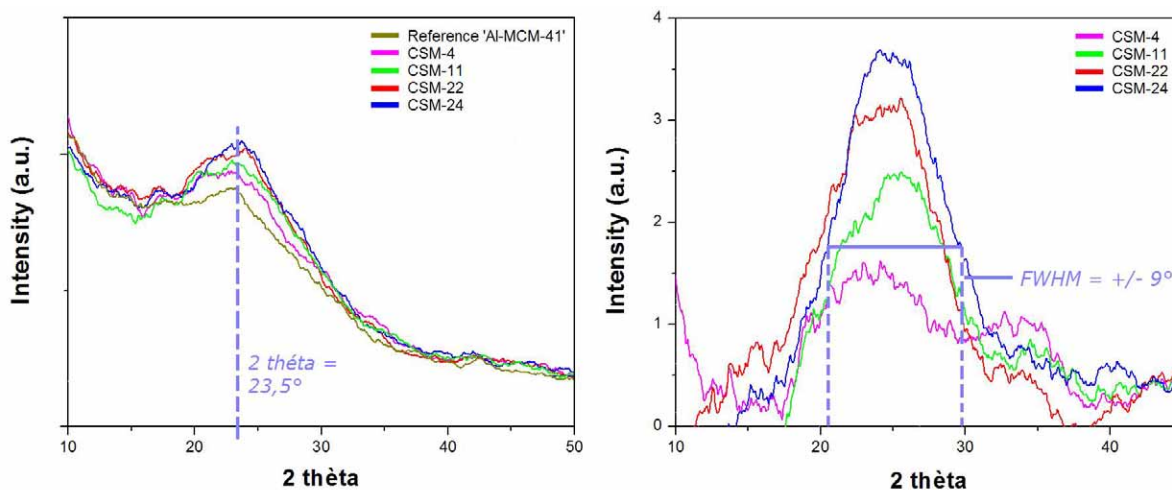


Figure 2: (left) XRD diffractograms of CSM and template materials (Al-MCM-41) in the range of 10° to 50° 2θ; (right) detailed overlay of the graphitic (002) diffraction peak at 23.5° 2θ

The mean crystallite size perpendicular to the graphene layers of the nano-graphite is estimated at 9.1 Angström.

Raman measurement

Identification of the carbon type, and determination of the mean crystallite size along the graphene layers of the intraporous nano-graphite are carried out by Raman spectroscopy.

The following data was extracted from a typical sample (CSM-23) as presented in **Figure 3**:

- Peak 1 position : 1354.1
- Peak 1 FWHM: 201.2
- Peak 1 Area: 754860
- Peak 2 position : 1590.6
- Peak 2 FWHM: 67.2

- Peak 2 Area: 297255
- I_D/I_G : 0.81

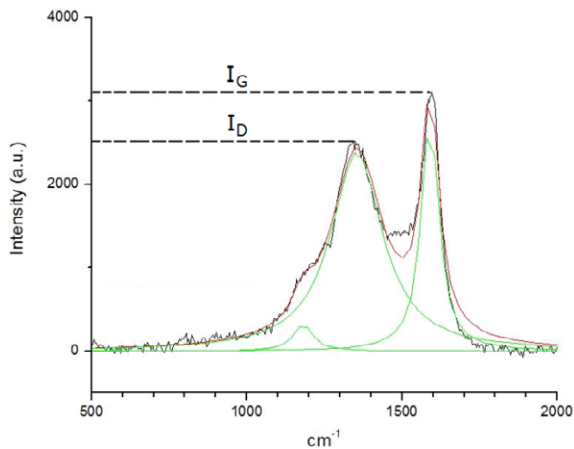


Figure 3: (black) Raman spectrum of CSM-23
 (green) Lorentz Plot of the Raman spectrum

Varying the excitation energy of the laser results in a blue shifting of the D-band position as presented in **Figure 4**. From the positions related to the excitation energy empiric data for the chemical shift can be calculated:

- $E = h \cdot v$ ($h = 6.626 \cdot 10^{-34} \text{ J.s}$)
- Energy of excitation source ($v = c / \lambda$) and $1.6021 \cdot 10^{-19} \text{ J} = 1 \text{ eV}$
 - 488 nm: $3.10^8 \text{ m.s}^{-1} / 488 \times 10^{-9} \text{ m} \rightarrow v = 6.148 \times 10^{14} \text{ s}^{-1} \rightarrow E = 4.073 \times 10^{-19} \text{ J} \rightarrow E (488\text{nm}) = 2.54 \text{ eV}$
 - 532 nm: $3.10^8 \text{ m.s}^{-1} / 532 \times 10^{-9} \text{ m} \rightarrow v = 5.639 \times 10^{14} \text{ s}^{-1} \rightarrow E = 3.736 \times 10^{-19} \text{ J} \rightarrow E (532\text{nm}) = 2.33 \text{ eV}$
 - 633 nm: $3.10^8 \text{ m.s}^{-1} / 633 \times 10^{-9} \text{ m} \rightarrow v = 4.739 \times 10^{14} \text{ s}^{-1} \rightarrow E = 3.140 \times 10^{-19} \text{ J} \rightarrow E (633\text{nm}) = 1.96 \text{ eV}$

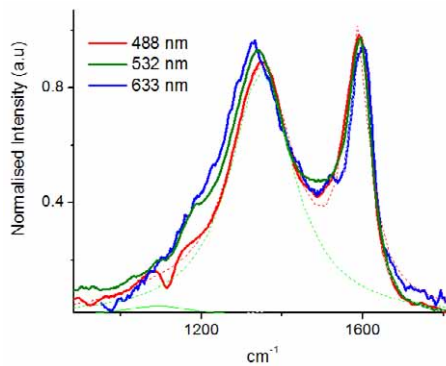


Figure 4: Illustration of D-band shifting according to laser energy.
 Raman spectra resulting from CSM-22 sample.

The dependence of the position of the D-band to the energy of the excitation wavelength as calculated from **Figure 4** is given as follows:

- 488 nm: 2.54 eV and 1352 cm^{-1}
- 532 nm: 2.33 eV and 1342 cm^{-1}
- 633 nm: 1.96 eV and 1328 cm^{-1}

The shift of the Raman signal per eV is characteristic of a disperse Raman band (see main text), and can be calculated by fitting these points by a linear relationship (correlation factor of 0.996) as illustrated in **Figure 5**. As such the Raman shift can be mathematically expressed as a shift of 41 cm^{-1} per eV in accordance with literature (ref. 12 in main text).

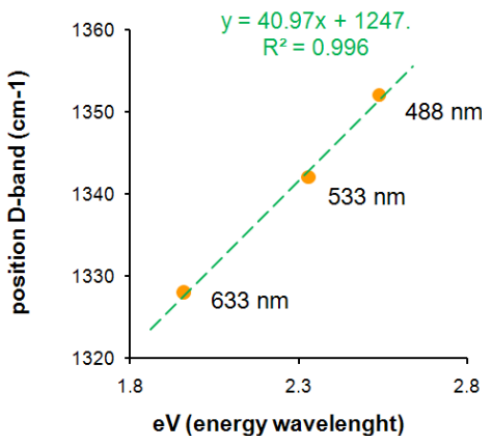


Figure 5: shift of the D-band with varying excitation wavelength

SEM and HRTEM visualization of CSM

SEM was performed on a Philips XL FEG30 equipment to visualize the morphology of the CSM samples before (**Figure 1**) and after impregnation and subsequent pyrolysis of the carbon precursor solution (**Figure 6, left**). For none of the CSM samples external amorphous carbon or graphite could be observed. SEM pictures of the particles after an HF treatment demonstrate the morphology is retained after dissolving the silica template and are given in **Figure 6** (right). As such this indicates the carbon originally resides mostly inside the pores of the template.

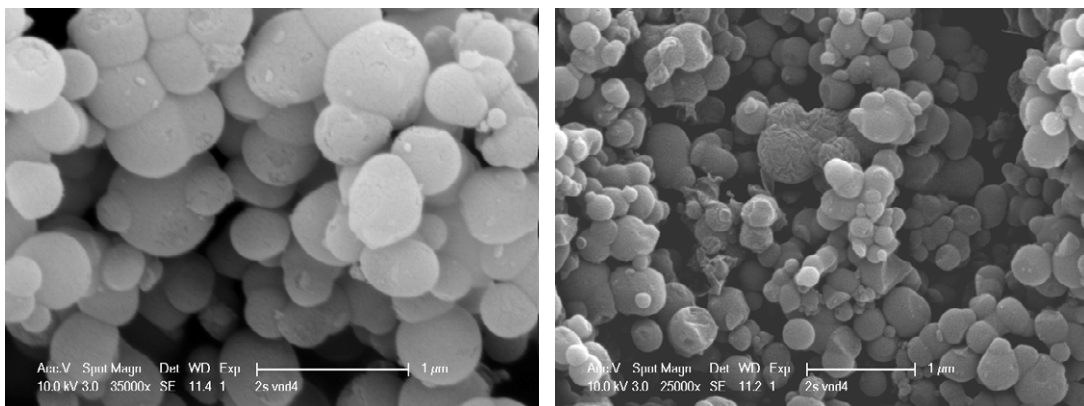


Figure 6: SEM image of (left) CSM-FA-1073-19 (right) pure carbon sample obtained from CSM-FA-1073-19 after removal of the silica template by HF treatment

The microcrystalline structure of the carbon of the CSM samples was examined by HRTEM. A FEI Tecnai G2 transmission electron microscope operating at 200kV was used. To avoid difficulties during the imaging due to the presence of the amorphous silica, the silica template was washed out of all samples examined with HF. In **Figure 7** we can clearly observe domains of carbon micro crystallites with an estimated length between 5 and 15 Angström. These values are well in the range of the 12 Angström calculated using Raman spectroscopy (see main text). Most micro crystallites exhibit 3 to 5 layers, which is consistent with the XRD observations (see main text) suggesting about 3 layers of graphene.

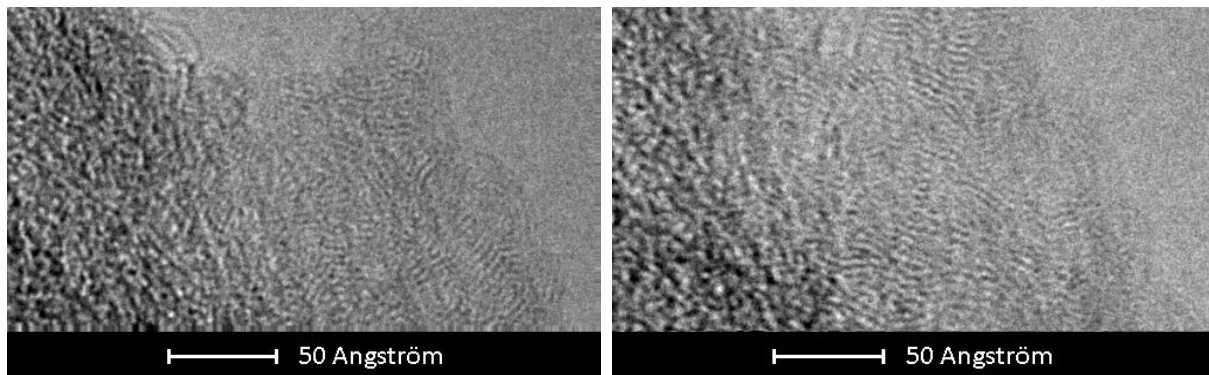


Figure 7: HRTEM images of an HF treated CSM-FA-1073-19 (pure carbon)

N₂ adsorption measurements

Nitrogen adsorption has been performed to examine the effect of the various carbon loadings on the overall pore volume and surface area characteristics of CSM samples. The change in pore volume has been illustrated (fig. 2 in main text). A complete summary of the N₂ sorption data has been listed in **Table 1**.

Table 1: Pore volume and surface area of CSM samples with various carbon loading ; * as calculated by the t-plot method

	Al-MCM-41	CSM-FA-1073-5	CSM-FA-1073-8.5	CSM-FA-1073-18.5	CSM-FA-1073-23.5	CSM-FA-1073-24.5
V _{micro} (cm ³ /g) *	0.000	0.000	0.075	0.135	0.165	0.230
V _{meso}	0.590	0.450	0.375	0.255	0.015	0.000
V _{tot}	0.590	0.450	0.450	0.390	0.180	0.230
S _{BET} (m ² /g)	1112	923	744	690	310	394
S _{meso/macropores} (m ² /g) *	1112	910	723	488	32	79

The heating rate during carbonisation of the FA impregnated MCM-41 samples is crucial in order to obtain the shape selective effect (see main text) in the carbon silica material (CSM). This is demonstrated in **Figure 8** by the three pore size distribution plots (according to the Horvath-Kawazoe model assuming slit-like pores and carbon) for three different heating rates: 1, 10 and 20°C min⁻¹. While a very narrow pore size distribution around 5.3 Angström was found for the slow heating rate, the distribution becomes broad to very broad upon heating faster during the carbonisation step.

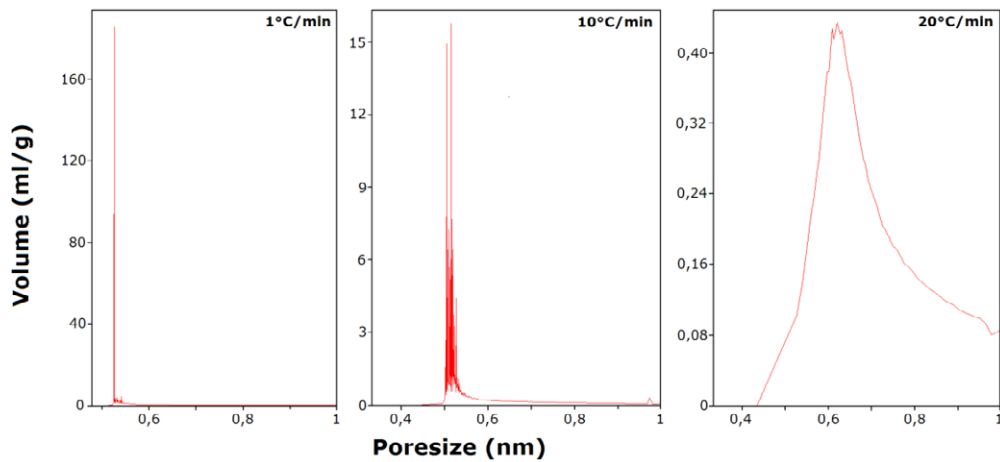


Figure 8: Pore size distribution of CSM-23 for different heating rates during pyrolysis (using Horvath-Kawazoe model assuming slit-like pores): (left) 1K/min: very narrow micropore distribution around 5.3 Ångström; (middle) 10K/min: slightly broader micropore distribution; (right) 20K/min: very broad micropore distribution.

Comparative study of adsorbents for linear branched paraffine separation

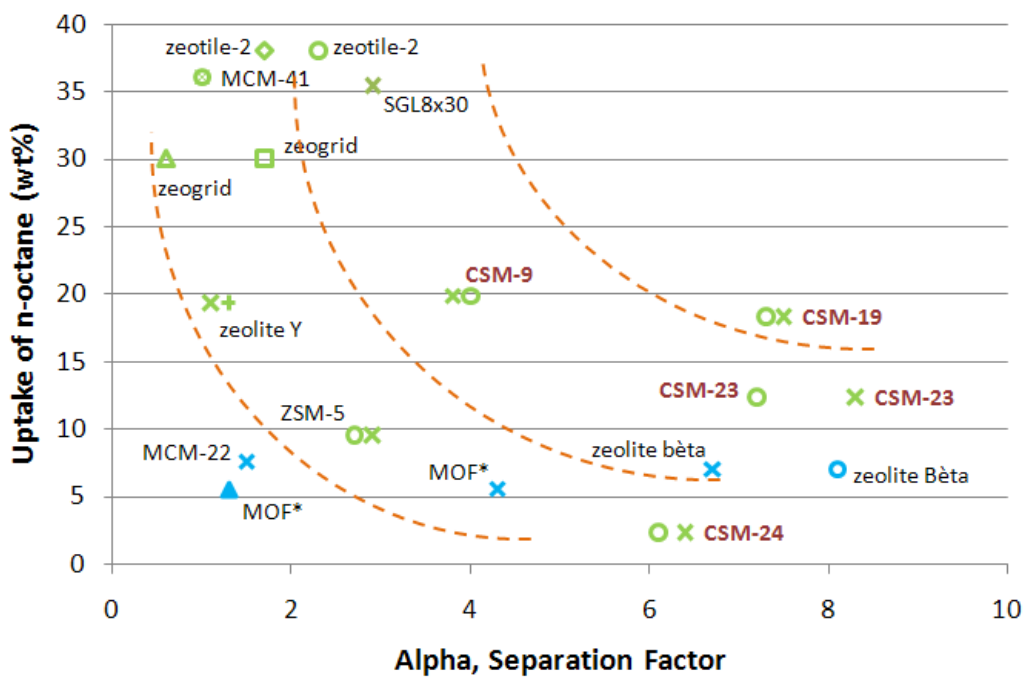


Figure 9: Comparison between typical sorbent materials based on: [X-axis] separation factor as determined by separation of: (X) 2,2-dimethylbutane and n-hexane, (Δ) 2-methylbutane and 2,2-dimethylbutane, (\square) 2,2,4-trimethylpentane and n-heptane, (\diamond) 2,3-dimethylbutane and n-hexane, (\circ) 3,3-dimethylpentane and n-heptane, (+) 2,3-dimethylpentane and n-heptane, (\blacktriangle) 3-methylpentane and n-hexane; [Y-axis] capacity as determined by n-octane uptake (green) and n-hexane uptake (blue). Own work materials are labeled in red.

Table 2: Overview of alpha values, capacities and experimental conditions of common adsorbentia and the entitled CSMs; n.d.: no data available; * capacity estimated using the adsorption isotherm and K'/L ; ** alpha values from chromatographic experiments with following temperature program: 393K (2min) / 393-433K (2 min) / 433K.

Adsorbent	Separation	Temp.	Alpha	Gravimetric	Temp.	Capacity	Reference
ZSM-5	22C4 / C6	573 K	2.9	octane	343K	9.5%	Denayer et al., J. Phys. Chem. B, Vol 102(23) (1998), 4588
ZSM-22	22C4 / C6	573 K	19.9	nonane	n.d.	4.0%	Ocakoglu et al., J. Phys. Chem B, 107 (2003), 398
Mordeniet	22C4 / C6	573 K	3.9	n.d.	n.d.	n.d.	Denayer et al., J. Phys. Chem. B, Vol 102(23) (1998), 4588
Zeolite Beta	22C4 / C6	573 K	6.7	hexane	423K	7.0%	Denayer et al., J. Phys. Chem. B, Vol 102(23) (1998), 4588
MCM-22	22C4 / C6	523 K	1.5	hexane	403K	7.5%	Denayer et al., J. Phys. Chem. B, Vol 110 (2006), 8551
Zeolite Y (Faujasite)	22C4 / C6	573 K	1.1	octane	598K	19.3%*	Denayer et al., Adsorption, Vol 3 (1997),
CSM-4	22C4 / C6	523 K	2.5	octane	333K	6.0%	own work
CSM-9	22C4 / C6	523 K	3.8	octane	333K	19.8%	own work
CSM-19	22C4 / C6	523 K	7.5	octane	333K	18.3%	own work
CSM-23	22C4 / C6	523 K	8.3	octane	333K	12.3%	own work
CSM-24	22C4 / C6	523 K	6.4	octane	333K	2.3%	own work
SGL8x30	22C4 / C6	523K	2.9	octane	333K	35.4%	own work
carboxen-569	22C4 / C6	523K	20.2	octane	333K	7.2%	own work
MCM-41	22C4 / C6	523 K	1.0	octane	333K	36.0%	own work
MCM-48	23C4 / C6	433 K	1.2	n.d.	n.d.	n.d.	Devriesse et al., Adv. Funct. Mater., Vol 17 (2007), 3911
MOF-508a	22C4 / C6	433 K	1.6	n.d.	n.d.	n.d.	Chen et al., Angew. Chem. Int. Ed., Vol 45 (2006), 1390**
Zn(BDC)(Dabco)0.5	22C4 / C6	n.d.	4.3	hexane	n.d.	5.5%	Garcia et al., J. Phys. Chem. B, Vol 111 (2007), 6101
Zeotile-2	23C4 / C6	433 K	1.7	octane	333K	38.0%	Devriesse et al., Adv. Funct. Mater., Vol 17 (2007), 3911
silicalite zeogrid	224C5 / C8	403 K	1.7	n.d.	n.d.	n.d.	Kremer et al., Adv. Funct. Mater., Vol 12(4) (2002), 286